
UrbanVLP: Multi-Granularity Vision-Language Pretraining for Urban Region Profiling

Xixuan Hao¹, Wei Chen¹, Yibo Yan¹, Siru Zhong¹, Kun Wang²,
Qingsong Wen³, Yuxuan Liang^{1*}

¹Hong Kong University of Science and Technology (Guangzhou)

²National University of Singapore ³Squirrel AI

{xhao390, wchen110, szhong691}@connect.hkust-gz.edu.cn, yuxliang@outlook.com,
{yanyibo70, qingsonedu}@gmail.com, wk520529@mail.ustc.edu.cn

Abstract

Urban region profiling aims to learn a low-dimensional representation of a given urban area while preserving its characteristics, such as demographics, infrastructure, and economic activities, for urban planning and development. However, prevalent pretrained models, particularly those reliant on satellite imagery, face dual challenges. Firstly, concentrating solely on macro-level patterns from satellite data may introduce bias, lacking nuanced details at micro levels, such as architectural details at a place. Secondly, the lack of interpretability in pretrained models limits their utility in providing transparent evidence for urban planning. In response to these issues, we devise a novel framework entitled UrbanVLP based on Vision-Language Pretraining. Our UrbanVLP seamlessly integrates multi-granularity information from both macro (satellite) and micro (street-view) levels, overcoming the limitations of prior pretrained models. Moreover, it introduces automatic text generation and calibration, elevating interpretability in downstream applications by producing high-quality text descriptions of urban imagery. Rigorous experiments conducted across six urban indicator prediction tasks underscore its superior performance.

1 Introduction

Urban Region Profiling, a scholarly endeavor within the domain of GeoAI [45, 54] and smart city [85], refers to the process of transforming urban regions into a low-dimensional vector representation using deep neural networks. Rooted in the escalating global prominence of urban environments and the imperative for urban planning, this academic discipline aims to capture and encode the multifaceted attributes of urban areas, such as demographic information, economic activity, environmental factors, infrastructure, and social dynamics, into a format that can be easily analyzed and utilized by computational models [73, 74]. Given the widespread accessibility of satellite imagery on platforms such as Google Maps [42, 51, 73], coupled with its wealth of information on regional features (*e.g.*, road networks, building density, and vegetation coverage), a predominant majority of initiatives *harness satellite imagery as the foundational modality* for learning urban region representations [88].

Through a comprehensive review of the current literature, we summarize mainstream methods for urban region profiling into two categories: **a) Task-specific supervised learning** commonly realizes urban region profiling in a fully supervised task, *e.g.*, identifying poverty levels [21, 59, 4, 5], crop yields [80, 70, 63, 57, 53, 78], and commercial activeness [24, 51]. However, its inherent task specificity (*i.e.*, reliant on ample labeled data), may impede the model’s capacity for broad generalization to other downstream tasks. **b) Vision pretraining**, also known as a type of Self-Supervised Learning [28], aims to learn general visual features from urban satellite imagery, which are subsequently fine-tuned on a specific task for enhancing performance [29, 6, 73, 51]. The inclusion

*Y. Liang is the corresponding author. Email: yuxliang@outlook.com

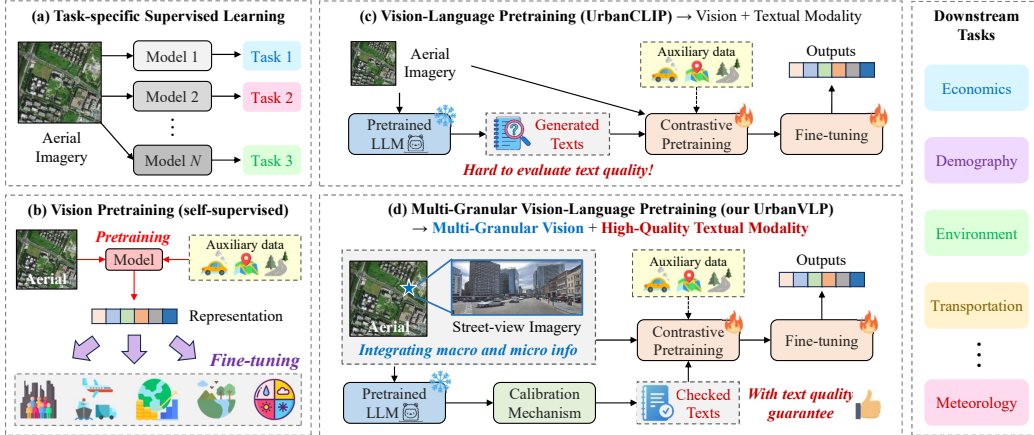


Figure 1: Frameworks for urban region profiling. Compared to existing literature, we present the first attempt to introduce multi-granular visual information and high-quality calibrated texts for this task.

of more auxiliary data, *e.g.*, Points of Interests (POIs) [19, 29, 82, 40], road networks [46, 47, 12] and human mobility [71, 64, 44, 39], leads to richer, more accurate, and more useful representations of urban areas. For clarity, Figure 1(a-b) depict a sketch of these two streams of approaches.

Despite the success of using satellite imagery for urban region profiling, urban environments exhibit a spatial hierarchy in reality, from a macro *region* level to a micro *location* level (*e.g.*, architectural details, street furniture). Previous approaches in Figure 1(a-b) mainly focus on single granularity, neglecting finer-grained visual clues. Nonetheless, as the saying goes, “*the devil is in the details.*”. By zooming into micro levels using corresponding street-view images, a more nuanced and fine-grained understanding emerges, as shown in the left hand side of Figure 1(d). Therefore, the integration and alignment of **multi-granularity information**, both macro-level and micro-level, remain ongoing challenges in urban region profiling that require further exploration.

Furthermore, while urban planners rely on explainable evidence for service deployment and urban planning, the vision-pretraining-based models for urban region profiling mostly **lack interpretability**. They typically learn a mapping from single/multi-modal data to the representations, posing a significant challenge in comprehending the intrinsic factors influencing the prediction outcomes. In light of the recent surge in Large Language Models (LLMs) [58, 84, 55], UrbanCLIP [74] stands out as an innovative solution, which effectively integrates textual modality as auxiliary knowledge into urban region profile, as depicted in Figure 1(c). However, the text generation process of UrbanCLIP raises several critical concerns. *i) Hallucination*: The generation of textual content sometimes deviates from or introduces information not present in the input satellite imagery. *ii) Homogenization*: The generated descriptions appear overly simplified and general, potentially leading to homogenization and inadequate differentiation. To better align with the intricacies of satellite (or street-view) imagery, *we necessitate a more powerful approach that goes beyond the intuitive text generation method in UrbanCLIP, ensuring a more faithful and explainable representation of urban regions.*

In this paper, we present a Vision-Language Pretraining framework (i.e., **UrbanVLP**) for urban region profiling. As depicted in Figure 1(d), our model elaborately integrates **multi-granularity information** from both satellite (macro-level) and street-view (micro-level) imagery to produce comprehensive urban region representations, while simultaneously harnessing the interpretability inherent in **high-quality textual descriptions**. Targeting the first challenge, we introduce a novel *Multi-Granularity Cross-Modal Alignment* module, which utilizes dual-branch contrastive learning to establish alignment between information derived from two semantic granularities. To address the second issue (*i.e.*, lack of interpretability), we devise an *Automatic Text Generation* together with a *Calibration* mechanism to uphold text quality standards. Given the impracticality of generating a large number of descriptions using GPT4V [75] or Gemini [18] due to prohibitive expense, we utilize a closely comparable GPT4V [75] model called ShareGPT4V [11]. To guarantee the quality of LLM-generated descriptions, we propose a reference-free metric called `PerceptionScore`, motivated by the human evaluation system.

In summary, our major contributions lie in the following aspects:

- *Multi-Granularity Cross-Modal Alignment.* We explore the role of two distinct visual data modalities at various semantic granularities – satellite imagery and street-view imagery. We integrate street-view data to inject fine-grained semantic information through token-level contrastive learning. By aggregating and fusing local features within a specific region with satellite imagery data, we facilitate the development of a robust and comprehensive representation of urban landscapes.
- *Automatic Text Generation and Calibration.* Powered by image-to-text LLMs, we generate text descriptions and implement a robust evaluation mechanism based on a newly-proposed reference-free metric, ensuring the fidelity between the generated texts and the corresponding image content.
- *Empirical Evidence.* We evaluate the proposed UrbanVLP on six urban indicator prediction tasks (e.g., GDP, population, and carbon emission) in diverse urban landscapes. Extensive experiments demonstrate that our UrbanVLP outperforms existing approaches by an average improvement of 3.95% on the R^2 metric, while preserving good interpretability based on generated text.
- *New Benchmark and System.* We will open-source the first multi-granular vision-text benchmark (CityScape) for urban region profiling upon paper notification, encompassing 6 downstream tasks. Moreover, we have deployed a web platform to verify the model’s practicality (see Appendix I).

2 Related work

We formally define the problem of urban region profiling. Given a satellite images I_g^{sa} , a set of street-view images \mathcal{I}_g^{sv} belonging to the target coverage, and their corresponding latitude and longitude pair \mathcal{L}_g . The objective is to employ a learning function \mathcal{F} to map them to representation vectors $\mathbf{e}_g = \mathcal{F}(I_g^{sa}, \mathcal{I}_g^{sv}, \mathcal{L}_g)$. The representation can then be further utilized in downstream tasks, such as inferring urban indicators \mathbf{Y}_g for any given region g . We assume that during the training phase, automated additional text descriptions are available. The detailed formulation and definitions related to this task are provided in Appendix A. Next, we introduce the related work from three aspects.

Urban Region Profiling. In literature, many studies have focused on learning task-specific region representations from various urban data, especially urban imagery due to its consistent updates and easy accessibility [41, 51, 73]. For example, Urban2Vec [72] integrated *street-view imagery* and POI data to learn neighborhood embeddings. Some contrastive learning approaches like PG-SimCLR [73] and UrbanCLIP [74] have shown success in representing urban regions through *satellite images*. However, the aforementioned works exclusively considered a single type of urban imagery, *overlooking the potential synergy between satellite imagery and street-view imagery, which can complement each other*. Recently, some efforts [7, 27, 41, 9, 33, 8, 27] have begun to explore the simple combination of satellite imagery and street-view imagery. Vision-LSTM [27] integrates diverse street-level images into the satellite image domain using an LSTM-based network for precise urban village identification. Li et al. [41] propose utilizing street segments for region modeling and predicting socio-economic indicators by merging street-view and satellite images through a multi-stage pipeline. Nevertheless, prior studies mostly overlook distinct features in satellite and street-view images for varied granularities. To this end, we propose a unified multi-granularity cross-modal alignment framework for comprehensive urban representation in this study.

Vision-Language Pretraining (VLP). VLP aims to jointly encode vision and language in a fusion model. Early works on VLP can be broadly categorized into single-stream [13, 31, 35] and two-stream [66, 52] methodologies, with the former using a unified architecture for modality integration and the latter employing separate encoders before merging modalities. Milestone work CLIP [61] and its variants [43, 76] highlight the efficacy of contrastive learning in cross-modal downstream tasks, such as zero-shot learning and cross-modal retrieval. Recent works [67, 2] shift towards leveraging LLMs knowledge for vision-language representation learning. *In urban region profiling, the potential of VLP paradigm remains untapped, with limited exploration of the benefits of textual information*. Our groundbreaking work introduces multiple types of text descriptions as supplements, aiming to learn more comprehensive and interpretable urban region representations.

Large Multimodal Model (LMM). As LLMs undergo rapid evolution, a faction within the research community is increasingly focused on integrating visual knowledge into these models, such as CLIP [61] and ALIGN [30]. Early studies [36, 37] enhanced CLIP with refined data strategies for more diverse datasets, which have proven effective for fundamental visual tasks [38, 50, 81] but have shown limitations for complex tasks such as visual question answering. Recently, new models like MiniGPT-4 [10], LLaVA [49], and InstructBLIP [14] have improved the understanding of complex problems by expanding parameters and training data, called large multimodal models (LMMs). In

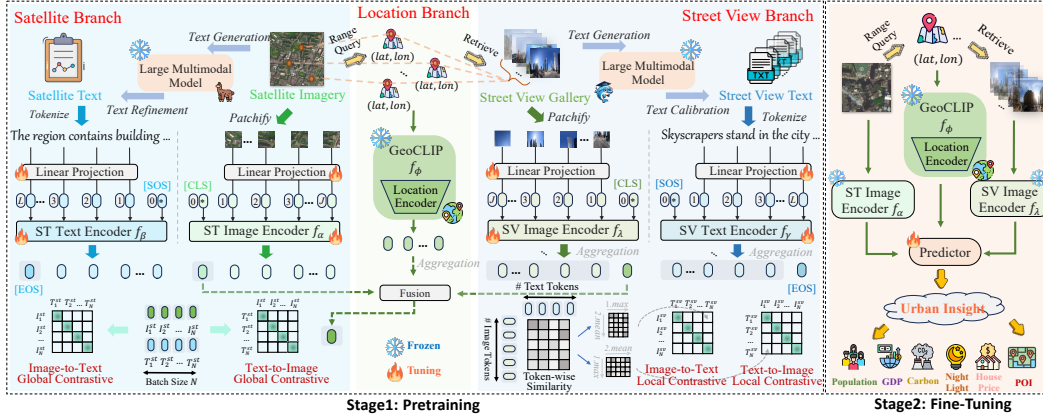


Figure 2: Overall framework of our proposed UrbanVLP.

this paper, we comprehensively evaluate the text generation quality of representative LMMs model and propose an automated text description generation and calibration technique to ensure effective image description capabilities with LMMs.

3 Methodology

We present an overview of our proposed framework in Figure 2, which is decoupled into two stages. In the pretraining stage, we devise an automatic text generation and calibration module using ShareGPT4V [11] to generate textual descriptions for street-view images with geographical and visual prompts. Introducing the PerceptionScore to ensure high-quality text, we then develop a multi-granularity cross-modal alignment framework through multi-level contrastive learning and fine-grained information injection. In the fine-tuning stage, we use frozen encoders from Stage 1 to extract data features, fine-tune a lightweight MLP for precise predictions, and incorporate optional street-view imagery and geographical coordinates to enrich the analysis.

3.1 Automatic Text Generation and Calibration

Text Generation. For each street-view image, we utilize advanced Large Multimodal Models (LMMs) due to their robust cross-modal knowledge storage capabilities, to provide comprehensive textual descriptions. However, this confronts two primary challenges. Firstly, due to substantial financial costs associated with API usage, employing closed source LMMs like GPT4V [75] or Gemini [18] for generating tens of thousands of text descriptions is impractical. Secondly, street-view images often encompass diverse detailed information, necessitating a well-designed prompt template for obtaining high-quality textual descriptions.

To address these issues, we first utilize a closely related GPT4V model, known as ShareGPT4V [11], to generate street-view image descriptions. This model is a powerful language model with vision capabilities trained on 100k GPT4V generated captions, demonstrating captioning capabilities comparable to GPT4V. In the process of designing text prompt templates, the proportion of segmented elements in street-view images reflects the distribution of elements, aiding LMMs in evaluating the importance of each element. To achieve this, we employ a pretrained segmentation model to decouple visual elements and calculate the proportion of segmentation for each element. Simultaneously, urban and geospatial coordinates of street-view images are included as prompts to guide the expression of additional urban information. Template and segmentation ratio details can be found in Appendix F.

Text Calibration. As existing works [32, 16, 74] demonstrated that the quality of the textual descriptions is crucial for enhancing model performance. However, previous research [74] primarily employed simplistic rules and manual refinement processes for text description of satellite images, leading to potential unresolved hallucination issues [62] in generated text descriptions. Besides, rule-based methods are overly general and fail to address specific issues in each image description as they are tailored to particular cases. On the other hand, manual rewriting is highly labor-intensive.

Therefore, an effective method for evaluating text quality and calibrating the alignment between text and image content is necessary to ensure a high level of LMM-inherent knowledge injection. In contrast to the common evaluation methods used to assess the quality of descriptions generated by

LMMs, which typically rely on manually annotated image descriptions as references [65, 83, 34] to measure content overlap, we introduce an automatic mechanism designed to simulate human evaluation systems. This mechanism places greater emphasis on semantic similarity rather than merely assessing typical content overlap, thereby introducing PerceptionScore as a novel quality metric. Specifically, it comprises two components: text semantic quality and visual recall quality. The former approach directly adopts the efficient implementation of CLIPScore [25], which is based on CLIP’s [61] strong zero-shot capabilities and demonstrates high correlation with human semantic judgment. However, CLIPScore solely provides a measure of textual quality and fails to indicate whether specific elements in the image are omitted in the text (visual recall) [26].

To address this problem, we propose CycleScore, a metric aimed at aligning fine-grained elemental information within the image I . As illustrated in Figure 3, given each description T generated by LMMs, we use the state-of-the-art open-sourced text-to-image model SDXL(\cdot) [60] to generate a consistent image I' , reflecting various information contained in the text intuitively. Subsequently, we use a pretrained segmentation model Seg(\cdot) [1] to decouple consistent semantic elements [17] in both the input and output images and calculate the Mean Absolute Error, *i.e.* MAE(\cdot) score, constraining visual-semantic consistency. We formalize the process as follows:

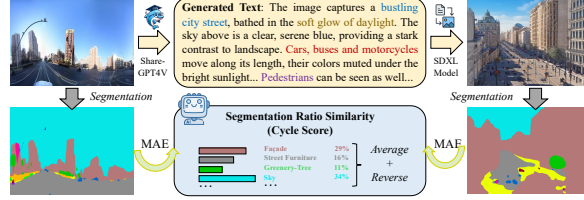


Figure 3: The procedure of CycleScore calculation.

$$\begin{aligned}
 I' &= \text{SDXL}(I), \quad \text{CycleScore}(I, I') = 1 - \text{MAE}(\text{Seg}(I), \text{Seg}(I')), \\
 \text{PerceptionScore}(I, T) &= (\text{CLIPScore}(I, T) + \text{CycleScore}(I, I'))/2.
 \end{aligned}
 \tag{1}$$

3.2 Multi-Granularity Cross-modal Alignment

Modality Representation. Utilizing automated generation techniques, we obtain a dataset of high-quality image-text pairs, represented as $D = (I, T)$. Here, I denotes satellite images I^{st} or street-view images I^{sv} , while T represents satellite text descriptions T^{st} or street-view text descriptions T^{sv} .

We first deploy Vision Transformer (ViT) [15] as an image encoder to process images derived from satellite and street-view sources. Finally, we use the output \mathbf{z}_l^0 corresponding to the special tokens I_{cls} inserted at the beginning as the final output of the image encoder, rewrite as \mathbf{z}_I for image representation. Concurrently, we use basic Transformer-Encoder [68] as a text encoder by default to comprehend and encode the semantics of textual descriptions in parallel. Furthermore, considering that the geospatial location information associated with street-view images can aid in pinpointing the precise geospatial coordinates of the area, we utilize the open-sourced GeoCLIP’s [69] location encoder to effectively instill geospatial information. This location encoder captures longitude and latitude \mathcal{L}_g , generating semantically rich, high-dimensional geospatial features, denoted as \mathbf{z}_L .

Modality Alignment. The efficient alignment of visual and textual modalities is crucial for accurately modeling regional representations at both the coarse-grained global level and the fine-grained local level. To capture global visual information, in addition to the overall visual features for the region derived from satellite images, the clustering aggregation of location-level clues gathered within the region can additionally inject fine-grained details. Therefore, we further incorporate fine-grained information from street-view images, which are simultaneously fused with the corresponding geographical features. This approach aids in learning a robust and comprehensive representation of urban areas. The formalized process is as follows:

$$\mathbf{z}_{gst} = f(\mathbf{z}_{I_{st}}, \text{Aggr}(\mathbf{z}_{I_{sv}}^1, \mathbf{z}_{I_{sv}}^2, \dots, \mathbf{z}_{I_{sv}}^m), \text{Aggr}(\mathbf{z}_L^1, \mathbf{z}_L^2, \dots, \mathbf{z}_L^m)),
 \tag{2}$$

where $\mathbf{z}_{I_{st}}$ represents the satellite visual features for the queried region, $\mathbf{z}_{I_{sv}}^k$ denotes the k -th street-view visual feature in that region, and \mathbf{z}_L^k represents the k -th street-view location feature in the same region. The variable m indicates the count of street-view scenes within the region. Aggr(\cdot) denotes the aggregation method. The function f signifies the feature fusion method.

To establish a global-level semantic correspondence between satellite visual data and their associated textual descriptions, we employ a joint contrastive optimization approach for the image and text modal encoders in the satellite branch. For the i -th satellite image-text pair (I_i^{st}, T_i^{st}) in a mini-batch, we contrast the image-text pairs against others in the samples, which aims to maximally preserve the mutual information between the authentic pairs in the latent space. The global contrastive loss

function \mathcal{L}_{CG} is composed of two terms: $\mathcal{L}_{CG}^{Image \rightarrow Text}$ and $\mathcal{L}_{CG}^{Text \rightarrow Image}$, which measure the similarity between the visual and textual embeddings, respectively, defined as: The global contrastive loss function \mathcal{L}_{CG} is composed of two terms which measure the similarity between the visual and textual embeddings, respectively, defined as:

$$\mathcal{L}_{CG} = -\frac{1}{N} \left(\sum_i^N \log \frac{\exp(I_{g_i}^\top T_{g_i} / \tau)}{\sum_{j=0}^N \exp(I_{g_i}^\top T_{g_j} / \tau)} + \sum_i^N \log \frac{\exp(T_{g_i}^\top I_{g_i} / \tau)}{\sum_{j=0}^N \exp(T_{g_i}^\top I_{g_j} / \tau)} \right), \quad (3)$$

where I_{g_i} and T_{g_j} are the normalized embedding of satellite representation $\mathbf{z}_{g_{st}}$ in the i -th pair and that of textual representation $\mathbf{z}_{T_{st}}$ in the j -th pair, respectively. Besides, N is the batch size, and τ is the temperature for contrastive learning.

For capturing the local-level information, given that the street-view branch is expected to capture fine-grained details to enrich region embedding at ground level, approaches like [61, 30] rely exclusively on the similarity of each modality’s global feature, thus lacking the capability to capture finer-level information such as the relationship between visual objects and textual tokens [76]. We leverage a fine-grained interaction mechanism to implement cross-modal alignment. Specifically, we utilize token-level maximum similarity between visual and textual tokens to direct the contrastive objective. Initially, we compute the similarity between each visual token and all textual tokens, and then leverage the maximum value to calculate the average similarity of all image tokens to textual tokens. The similar approach is also applied to text-to-image.

$$\text{SIM}(v_i, t_i) = \frac{1}{l_1} \left(\sum_{k_1=1}^{l_1} \text{argmax}_{k_2 \in [0, l_2)} (v_{ik_1}^\top t_{ik_2}) \right), \quad (4)$$

$$\text{SIM}(t_i, v_i) = \frac{1}{l_2} \left(\sum_{k_2=1}^{l_2} \text{argmax}_{k_1 \in [0, l_1)} (t_{ik_2}^\top v_{ik_1}) \right), \quad (5)$$

where v_i and t_j denote the normalized embedding of street-view representation $\mathbf{z}_{I_{sv}}$ in the i -th pair and that of textual representation $\mathbf{z}_{T_{sv}}$ in the j -th pair, respectively. The fine-grained token-level representation can be optimized through:

$$\mathcal{L}_{CL} = -\frac{1}{N} \left(\sum_i^N \log \frac{\exp(\text{SIM}(v_i^\top, t_i) / \tau)}{\sum_{j=0}^N \exp(\text{SIM}(v_i^\top, t_j) / \tau)} + \sum_i^N \log \frac{\exp(\text{SIM}(t_i^\top, v_i) / \tau)}{\sum_{j=0}^N \exp(\text{SIM}(t_i^\top, v_j) / \tau)} \right). \quad (6)$$

3.3 Pretraining & Fine-Tuning

Pretraining Stage. The overall objective of UrbanVLP can be defined as the simultaneous optimization of the aforementioned two losses:

$$\mathcal{L}_{Total} = \alpha \mathcal{L}_{CG} + \beta \mathcal{L}_{CL}. \quad (7)$$

where α and β are weight hyperparameter. Through backpropagation optimization, We achieve multi-granularity cross-modal urban image-text input data alignment, resulting in a robust encoder.

Fine-Tuning Stage. During the fine-tuning stage, we employ a linear probing approach [23]. This process begins by extracting frozen features \mathbf{e}_{st} , \mathbf{e}_{sv} , \mathbf{e}_p from the pretrained encoder for satellite images, street-view images, and street-view positions (The latter two are optional). Subsequently, these features are fused, and a minimalist classifier (MLP) is trained on top to fine-tune the prediction of urban metrics, denoted as $\mathbf{Y}_i = MLP(\mathbf{e}_{sa}, \mathbf{e}_{sv}, \mathbf{e}_p)$. As depicted in Figure 2, these encoders have adapted to capturing high-level abstractions from extensive visual data, enabling the MLP to manipulate static features and study the model’s inference capabilities. Note that in downstream tasks, text information is unnecessary as additional text generation time impedes real-time application.

4 Experiments

4.1 Experimental Setup

Dataset & Task Description.

In this paper, given the current lack of open-sourced datasets in the research community, we introduce a new benchmark dataset named CityScape, which will be released upon paper notification. CityScape is unique in that it comprises a dual-category structure encompassing both satellite and street-view image components, each paired with corresponding high-quality textual descriptions. For the satellite image-text pairs, we adhere to [74] to utilize core area data of four cities in China. A comprehensive overview of CityScape, along with relevant statistics, is provided in Appendix B.

Table 1: Urban indicators prediction results in four datasets. The best results are in bold and the second-best results are underlined.

Methods	UrbanVLP			StructuralUrban [41]			Vision-LSTM [27]			UrbanCLIP-SV [74]			UrbanCLIP [74]			PG-SimCLR [73]			ViT [15]			
	Metric	R ²	RMSE	MAE	R ²	RMSE	MAE	R ²	RMSE	MAE	R ²	RMSE	MAE	R ²	RMSE	MAE	R ²	RMSE	MAE			
Beijing	Carbon	0.769	0.477	0.369	<u>0.736</u>	<u>0.518</u>	<u>0.405</u>	0.674	0.519	0.433	0.489	0.713	0.548	0.703	0.541	0.539	0.430	0.797	0.632	0.411	0.810	0.607
	Population	0.714	0.523	0.411	<u>0.691</u>	<u>0.545</u>	<u>0.427</u>	0.640	0.591	0.518	0.435	0.734	0.581	0.655	0.576	0.459	0.476	1.228	0.963	0.442	0.861	0.635
	GDP	0.537	0.684	0.416	<u>0.512</u>	<u>0.694</u>	<u>0.426</u>	0.497	0.717	0.469	0.188	0.910	0.568	<u>0.514</u>	0.694	0.445	0.270	1.679	1.067	0.265	1.073	0.730
	Night Light	0.470	0.668	0.403	<u>0.421</u>	<u>0.696</u>	<u>0.459</u>	0.354	0.747	0.475	0.304	0.769	0.483	0.377	0.741	0.468	0.367	0.728	<u>0.404</u>	0.358	0.733	0.523
	House Price	0.503	0.644	0.482	<u>0.493</u>	<u>0.649</u>	<u>0.485</u>	0.471	0.658	0.495	0.451	0.674	0.515	<u>0.501</u>	<u>0.647</u>	0.486	0.341	0.718	<u>0.555</u>	0.332	0.719	0.569
	POI	0.299	0.723	0.374	<u>0.275</u>	<u>0.725</u>	<u>0.380</u>	0.235	0.728	0.388	0.226	0.729	0.407	0.251	0.734	0.385	-	-	-	0.215	0.742	0.411
Shanghai	Carbon	0.718	0.520	0.381	<u>0.678</u>	0.550	0.432	0.571	0.606	0.455	0.576	0.465	0.450	0.673	0.560	<u>0.426</u>	0.270	0.742	0.551	0.254	0.758	0.522
	Population	0.589	0.609	0.476	<u>0.545</u>	<u>0.631</u>	<u>0.488</u>	0.518	0.659	0.522	0.400	0.793	0.592	0.533	0.650	0.511	0.288	1.051	0.831	0.279	0.826	0.627
	GDP	0.323	<u>0.805</u>	<u>0.593</u>	0.312	0.840	0.613	0.311	1.008	0.661	<u>0.323</u>	1.214	0.741	0.334	0.804	0.586	0.270	1.679	1.067	0.263	1.221	0.735
	Night Light	0.435	0.683	0.490	<u>0.411</u>	<u>0.690</u>	<u>0.497</u>	0.352	0.734	0.550	0.274	0.765	0.556	0.384	0.710	0.515	0.228	0.756	<u>0.495</u>	0.209	0.768	0.561
	House Price	0.381	0.680	0.386	<u>0.375</u>	<u>0.685</u>	<u>0.392</u>	0.246	0.704	0.390	0.240	0.711	0.402	0.265	0.710	0.395	-	-	-	0.234	0.713	0.406
	POI	0.701	0.513	0.372	<u>0.655</u>	0.550	0.404	0.554	0.564	0.457	0.425	<u>0.520</u>	0.473	0.585	0.603	<u>0.440</u>	0.413	0.951	0.716	0.374	0.665	0.528
Guangzhou	Carbon	0.655	0.573	0.454	<u>0.631</u>	<u>0.587</u>	<u>0.459</u>	0.614	0.619	0.509	0.491	0.693	0.622	0.627	0.596	0.473	0.294	1.046	2.112	0.263	0.821	0.661
	Population	0.442	<u>0.755</u>	<u>0.541</u>	0.429	0.781	0.549	0.412	0.997	0.624	0.327	0.998	0.690	0.446	0.752	<u>0.546</u>	0.263	1.157	1.553	0.249	1.122	0.719
	GDP	0.548	0.594	0.428	<u>0.508</u>	<u>0.607</u>	<u>0.448</u>	0.381	1.021	0.629	0.314	0.692	0.524	0.463	0.651	0.483	0.436	0.649	<u>0.432</u>	0.357	0.642	0.505
	Night Light	0.438	0.732	0.333	<u>0.357</u>	<u>0.758</u>	<u>0.359</u>	0.175	0.811	0.401	0.169	0.826	0.405	0.185	0.802	0.401	-	-	-	0.136	0.904	0.427
	House Price	0.625	0.605	0.464	<u>0.587</u>	<u>0.593</u>	<u>0.481</u>	0.534	0.609	0.516	0.460	0.621	0.529	0.541	0.607	0.526	0.234	0.975	0.746	0.221	0.727	0.574
	POI	0.790	0.452	0.348	0.724	0.476	0.386	0.624	0.562	0.471	0.589	0.604	0.484	<u>0.727</u>	0.510	0.392	0.294	1.046	2.112	0.280	0.832	0.654
Shenzhen	Carbon	0.533	0.682	0.447	<u>0.489</u>	<u>0.697</u>	<u>0.471</u>	0.462	0.723	0.517	0.433	0.755	0.577	<u>0.508</u>	<u>0.693</u>	<u>0.464</u>	0.294	1.046	2.112	0.254	1.226	0.779
	Population	0.457	0.667	0.459	<u>0.421</u>	<u>0.694</u>	<u>0.502</u>	0.404	0.702	0.508	0.320	0.717	0.531	0.387	0.709	0.511	0.247	0.934	0.738	0.254	0.715	0.530
	GDP	0.461	0.752	0.370	<u>0.321</u>	<u>0.780</u>	<u>0.389</u>	0.254	0.795	0.412	0.147	0.849	0.453	0.185	0.838	0.436	-	-	-	0.137	0.954	0.455
	Night Light	0.625	0.605	0.464	<u>0.587</u>	<u>0.593</u>	<u>0.481</u>	0.534	0.609	0.516	0.460	0.621	0.529	0.541	0.607	0.526	0.234	0.975	0.746	0.221	0.727	0.574
	House Price	0.790	0.452	0.348	0.724	0.476	0.386	0.624	0.562	0.471	0.589	0.604	0.484	<u>0.727</u>	0.510	0.392	0.294	1.046	2.112	0.280	0.832	0.654
	POI	0.457	0.667	0.459	<u>0.421</u>	<u>0.694</u>	<u>0.502</u>	0.404	0.702	0.508	0.320	0.717	0.531	0.387	0.709	0.511	0.247	0.934	0.738	0.254	0.715	0.530
1 st Count		56			1			0			1			5			0			0		

Baselines for Comparison. We compare our method with seven recent baselines in the field of urban imagery-based socioeconomic prediction. The single granularity imagery-based urban region representation learning methods include: **ViT** [15], **PG-SimCLR** [73], **UrbanCLIP** [74], **UrbanCLIP-SV** [74]. We also apply multiple baselines for multi-granularity urban imagery-based representation learning: **Vision-LSTM** [27] and **StructuralUrban** [41]. The in-depth overview of each baseline method is presented in the Appendix C.

Evaluation Metrics. The performance of our predictions is evaluated using a trio of standard metrics: the coefficient of determination denoted as R^2 , the root mean squared error (RMSE), and the mean absolute error (MAE). An increase in R^2 , along with a decrease in RMSE and MAE values, signifies improved model accuracy. More implementation details are provided in Appendix D.

4.2 Performance Evaluation

To further validate the effectiveness of the proposed UrbanVLP framework, we conduct comparisons with existing state-of-the-art methods on our proposed datasets. The comprehensive results are presented in Table 1, and we can draw the following conclusions: **UrbanVLP significantly surpasses the performance of baseline methods employing both single-granularity and multi-granularity imagery, achieving a substantial margin of improvement.** It can be seen that UrbanVLP outperforms the best baseline, StructuralUrban [41], by 3.3%, 2.3%, 2.5%, 4.9%, 1.0% and 2.4% in terms of R^2 for all 6 indicators: *Carbon*, *Population*, *GDP*, *Night Light*, *House Price* and *POI* in Beijing. The similar performance improvement can also be seen in the dataset of the other three cities. Besides, the average performance gain of UrbanVLP on RMSE and MAE in Beijing dataset are 1.8% and 2.1%, respectively. In order to provide a more intuitive display, we have created Radar Images in Figure 4 to visualize the performance of Beijing. The results further prove the effectiveness of our framework for urban region representation learning.

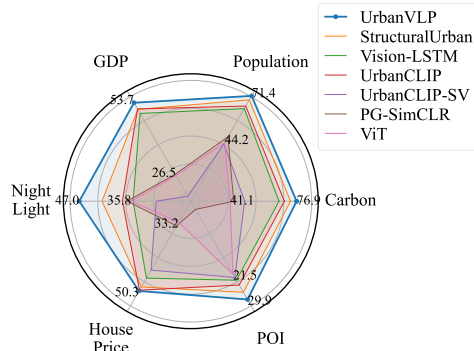


Figure 4: R^2 results in Beijing.

Multi-granularity cross-modal alignment effectively incorporates fine-grained information, demonstrating superior performance. We can observe that pipelines leveraging multi-granularity approaches typically demonstrate superior performance compared to those employing a single granularity level. This enhancement can be rationalized by the incorporation of additional fine-grained information derived from street-view imagery. Concurrently, it is noticed that UrbanCLIP-SV underperforms compared to UrbanCLIP, demonstrating that street-view imagery, while rich in fine-grained details, lacks macroscopic perspective, leading to suboptimal outcomes when used in isolation. This also underscores the irreplaceability of satellite imagery as a macroscopic visual modality.

Compared to other modalities, the textual modality facilitates a more explicit and comprehensive understanding of the region. In baseline models, there are works such as Vision-LSTM [27], which introduces trajectories, and PGSimCLR [73], which incorporates POI distributions to integrate external information and enhance regional representations. However, the superior performance of our UrbanVLP illustrates the efficacy of textual mobility as a high-information-density modality [23], which fully leverages the inherent knowledge of LLMs and explicitly enhances interpretability.

4.3 Ablation Studies

We conduct ablation studies to investigate the effectiveness of different components in UrbanVLP on Beijing dataset, including the Satellite branch (ST branch), Street-View branch (SV branch), and Location Encoding branch (LE branch). More ablation experiments can be found in Appendix H.

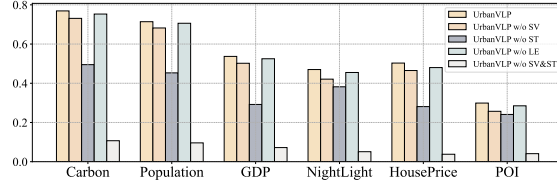


Figure 5: Ablation study on CityScape-Beijing.

The effectiveness of incorporating street-view branch. One of the main contributions of this work is the incorporation of multi-granularity information that reflects the urban spatial hierarchy. The street-view branch specifically represents micro-level modeling. It can be observed that the incorporation of street-view branch results in an average improvement of 3.56% in terms of R^2 . The presence of the street-view branch introduces the capture of rich detailed information, thereby enhancing the precision of the modeling. Furthermore, it is also can be seen that while street-view imagery provides fine-grained clues, its individual impact is still overshadowed by that of satellite imagery. This aligns with the performance differential between UrbanCLIP and UrbanCLIP-SV discussed in the Section 4.2, underscoring the indispensable role of macro-level modeling

The effectiveness of textual modality. In Table 1, we demonstrate the function of the textual modality by comparing UrbanVLP with a standard ViT-based model, which shares the same configuration as the unimodal visual encoder of UrbanVLP (encompassing both satellite and street-view branches). We then utilize the visual features extracted without textual augmentation to predict downstream urban indicators. As we can see, the lack of textual information leads to substantial performance degradation, underscoring the critical role of textual modalities in attaining a comprehensive visual representation. Similar findings were also reported in [74].

Exploration of the impact of location coordinates. The role of location coordinates has been underexplored in previous work of urban region representation learning. However, its importance has already been emphasized in work related to Geo-Localization [69, 79, 3]. In Figure 5, we evaluate the performance of the model without the Location Encoding branch. Although not as impactful as visual modalities, the inclusion of geospatial locations has yielded an average improvement of 1.5% in R^2 . However, when relying solely on location information, the performance is suboptimal. This indicates that at the current stage, location data can only serve as an auxiliary enhancement and lacks the capacity for standalone modeling due to its deficiency in contextual semantic information.

4.4 Qualitative Analysis

We further investigate the quality of generated texts and the predictive performance of UrbanVLP in practice. Due to page limitations, more experimental analysis can be found in the Appendix.

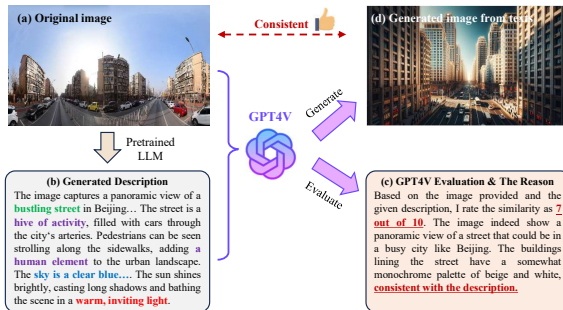
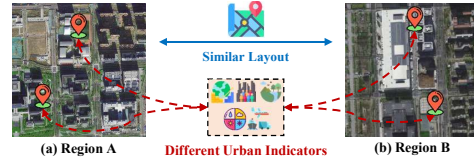


Figure 6: Illustration of the quality of our generated description example.



(c) Ground truth and prediction results of our UrbanVLP

Methods	Carbon		GDP		Population		House Price		Night Light	
	(a)	(b)	(a)	(b)	(a)	(b)	(a)	(b)	(a)	(b)
Ground Truth	550	4323	5235	10000	4727	6290	35776	56885	30	22
UrbanCLIP	488	1250	3207	5458	4511	4783	34123	39020	35	33
UrbanVLP	584	3730	5741	8743	4830	5815	37740	56885	33	25

Figure 7: Examples of predictions from UrbanCLIP and our proposed UrbanVLP.

Illustration of the quality of our generated descriptions. To visually illustrate the quality of the generated description, we present an example in Figure 6. The generated description of the street-view image (a) is depicted in (b). Subsequently, we employ GPT4V [75] to assess the quality score of the generated description, which is rated as 7 out of 10, indicating the effectiveness of the generated text. Furthermore, GPT4V also provides specific areas for improvement in (c). In (d), we utilize GPT4V to generate an image based on the description in (b). It is evident that the generated image bears a resemblance to the original one.

Case Study for Predicted Results. Here we also show some predicted results in Figure 7 on CityScape-Beijing dataset. As we can see, satellite images (a) and (b), although sharing similar layouts, differ significantly in their land use. (a) encompasses residential and campus areas, whereas (b) is indicative of industrial zones. Their socio-economic characteristics are entirely different, which could be reflected by socio-economic indicators. The carbon emissions and GDP of campus and residential area are significantly lower than those of industrial park, whereas the disparities in population and housing prices are not as pronounced, possibly due to the unique characteristics of school district housing near educational institutions. Night light intensity is similar across the two area due to the fact that the majority of nocturnal economic activities within factories occur indoors, unlike in Central Business Districts (CBDs) where extensive illumination is generated. The same principle applies to school and residential area as well. As observed, the predictions made by UrbanCLIP do not effectively differentiate between the two, with the downstream metrics in Figure 7(b) still inclined towards predicting a homogenized socio-economic functional area similar to that of (a). In contrast, the results from UrbanVLP are capable of distinctly distinguishing the socio-economic attributes of the two in terms of carbon emission, GDP, and house price. To showcase practical applications, we further develop a web-based system (Figure 8 and 17), with more details and discussion in Appendix I.



Figure 8: Our web platform. Zoom in or see Figure 17 for a better view.

Visualization of Region Representations. In this section, we map the region representations learned in UrbanVLP into a two-dimensional space using the PCA algorithm in Figure 9. This process aims to visualize how the semantic meanings of the regions are manifested within the high-dimensional representation space. As we can see, the three images on the left and on the right belong to different clusters, each exhibiting intra-cluster similarities and inter-cluster differences. Specifically, UrbanVLP effectively models regions into high-dimensional space, wherein satellite images with similar architectural layouts demonstrate spatial similarity. Consequently, this leads to a reasonable, accurate, and semantically rich representation of the regions.

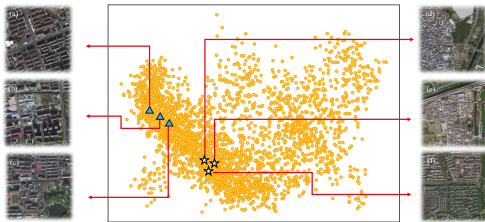


Figure 9: Representation space visualization.

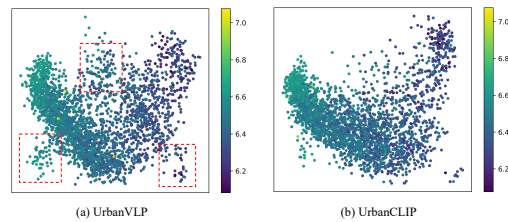


Figure 10: PCA visualization of urban imagery.

Figure 10 provides a further visualization with a population indicator, compared to UrbanCLIP. We use the dot color to indicate the population (log) in the corresponding regions of Beijing. As shown by the red dashed box, the regions modeled by UrbanVLP exhibit more significant clustering characteristics and greater distinction in high-dimensional space. Additionally, the lower parts of the two main band-shaped branches in the figure are also more distinctly separated. Points that are spatially close also have similar population values.

5 Conclusion and Future Work

Urban region representation learning plays a significant role in helping us understand the patterns, structures, and dynamics of cities. UrbanVLP, for the first time, explores the differences between

street-view and satellite images from a semantic granularity perspective, as well as their roles in modeling urban region representation. A text generation and calibration mechanism is also proposed to ensure high-quality description generation. It has achieved state-of-the-art results on the constructed CityScape and downstream dataset. In the future, the further research direction can be two-fold: 1) Adding additional modalities such as POIs to enhance information richness, and 2) enabling the design of better model architectures such as MAE [23] to efficiently utilize existing data source.

References

- [1] GitHub - CSAILVision/semantic-segmentation-pytorch: Pytorch implementation for Semantic Segmentation/Scene Parsing on MIT ADE20K dataset — github.com. <https://github.com/CSAILVision/semantic-segmentation-pytorch>. [Accessed 22-05-2024].
- [2] Jean-Baptiste Alayrac, Jeff Donahue, Pauline Luc, Antoine Miech, Iain Barr, Yana Hasson, Karel Lenc, Arthur Mensch, Katherine Millican, Malcolm Reynolds, et al. Flamingo: a visual language model for few-shot learning. *Advances in Neural Information Processing Systems*, 35: 23716–23736, 2022.
- [3] Guillaume Astruc, Nicolas Dufour, Ioannis Siglidis, Constantin Aronssohn, Nacim Bouia, Stephanie Fu, Romain Loiseau, Van Nguyen Nguyen, Charles Raude, Elliot Vincent, et al. Openstreetview-5m: The many roads to global visual geolocation. *arXiv preprint arXiv:2404.18873*, 2024.
- [4] Kumar Ayush, Burak Uz kent, Marshall Burke, David Lobell, and Stefano Ermon. Generating interpretable poverty maps using object detection in satellite images. *arXiv preprint arXiv:2002.01612*, 2020.
- [5] Kumar Ayush, Burak Uz kent, Kumar Tanmay, Marshall Burke, David Lobell, and Stefano Ermon. Efficient poverty mapping from high resolution remote sensing images. In *Proceedings of the AAAI Conference on Artificial Intelligence*, volume 35, pages 12–20, 2021.
- [6] Lubin Bai, Weiming Huang, Xiuyuan Zhang, Shihong Du, Gao Cong, Haoyu Wang, and Bo Liu. Geographic mapping with unsupervised multi-modal representation learning from vhr images and pois. *ISPRS Journal of Photogrammetry and Remote Sensing*, 201:193–208, 2023. ISSN 0924-2716. doi: <https://doi.org/10.1016/j.isprsjprs.2023.05.006>. URL <https://www.sciencedirect.com/science/article/pii/S0924271623001235>.
- [7] Elena Barbierato, Iacopo Bernetti, Irene Capecchi, and Claudio Saragosa. Integrating remote sensing and street view images to quantify urban forest ecosystem services. *Remote Sensing*, 12(2), 2020. ISSN 2072-4292. doi: 10.3390/rs12020329. URL <https://www.mdpi.com/2072-4292/12/2/329>.
- [8] Rui Cao, Jiasong Zhu, Wei Tu, Qingquan Li, Jinzhou Cao, Bozhi Liu, Qian Zhang, and Guoping Qiu. Integrating aerial and street view images for urban land use classification. *Remote Sensing*, 10(10):1553, 2018.
- [9] Rui Cao, Cai Liao, Qing Li, Wei Tu, Rui Zhu, Nianxue Luo, Guoping Qiu, and Wenzhong Shi. Integrating satellite and street-level images for local climate zone mapping. *International Journal of Applied Earth Observation and Geoinformation*, 119:103323, 2023. ISSN 1569-8432. doi: <https://doi.org/10.1016/j.jag.2023.103323>. URL <https://www.sciencedirect.com/science/article/pii/S1569843223001450>.
- [10] Jun Chen, Deyao Zhu, Xiaoqian Shen, Xiang Li, Zechun Liu, Pengchuan Zhang, Raghuraman Krishnamoorthi, Vikas Chandra, Yunyang Xiong, and Mohamed Elhoseiny. Minigtpt-v2: large language model as a unified interface for vision-language multi-task learning. *arXiv preprint arXiv:2310.09478*, 2023.
- [11] Lin Chen, Jisong Li, Xiaoyi Dong, Pan Zhang, Conghui He, Jiaqi Wang, Feng Zhao, and Dahua Lin. Sharegpt4v: Improving large multi-modal models with better captions. *arXiv preprint arXiv:2311.12793*, 2023.

- [12] Wei Chen, Chao Huang, Yanwei Yu, Yongguo Jiang, and Junyu Dong. Trajectory-user linking via hierarchical spatio-temporal attention networks. *ACM Transactions on Knowledge Discovery from Data*, 18(4):1–22, 2024.
- [13] Yen-Chun Chen, Linjie Li, Licheng Yu, Ahmed El Kholy, Faisal Ahmed, Zhe Gan, Yu Cheng, and Jingjing Liu. Uniter: Universal image-text representation learning. In *European conference on computer vision*, pages 104–120. Springer, 2020.
- [14] Wenliang Dai, Junnan Li, Dongxu Li, Anthony Meng Huat Tiong, Junqi Zhao, Weisheng Wang, Boyang Li, Pascale Fung, and Steven Hoi. Instructblip: Towards general-purpose vision-language models with instruction tuning, 2023.
- [15] Alexey Dosovitskiy, Lucas Beyer, Alexander Kolesnikov, Dirk Weissenborn, Xiaohua Zhai, Thomas Unterthiner, Mostafa Dehghani, Matthias Minderer, Georg Heigold, Sylvain Gelly, Jakob Uszkoreit, and Neil Houlsby. An image is worth 16x16 words: Transformers for image recognition at scale. In *International Conference on Learning Representations*, 2021. URL <https://openreview.net/forum?id=YicbFdNTTy>.
- [16] Lijie Fan, Dilip Krishnan, Phillip Isola, Dina Katabi, and Yonglong Tian. Improving clip training with language rewrites. In *NeurIPS*, 2023.
- [17] Zhuangyuan Fan, Fan Zhang, Becky PY Loo, and Carlo Ratti. Urban visual intelligence: Uncovering hidden city profiles with street view images. *Proceedings of the National Academy of Sciences*, 120(27):e2220417120, 2023.
- [18] Chaoyou Fu, Renrui Zhang, Haojia Lin, Zihan Wang, Timin Gao, Yongdong Luo, Yubo Huang, Zhengye Zhang, Longtian Qiu, Gaoxiang Ye, et al. A challenger to gpt-4v? early explorations of gemini in visual expertise. *arXiv preprint arXiv:2312.12436*, 2023.
- [19] Yanjie Fu, Pengyang Wang, Jiadi Du, Le Wu, and Xiaolin Li. Efficient region embedding with multi-view spatial networks: A perspective of locality-constrained spatial autocorrelations. In *Proceedings of the AAAI Conference on Artificial Intelligence*, volume 33, pages 906–913, 2019.
- [20] Peng Gao, Jiaming Han, Renrui Zhang, Ziyi Lin, Shijie Geng, Aojun Zhou, Wei Zhang, Pan Lu, Conghui He, Xiangyu Yue, et al. Llama-adapter v2: Parameter-efficient visual instruction model. *arXiv preprint arXiv:2304.15010*, 2023.
- [21] Sungwon Han, Donghyun Ahn, Sungwon Park, Jeesurk Yang, Susang Lee, Jihee Kim, Hyunjoon Yang, Sangyoon Park, and Meeyoung Cha. Learning to score economic development from satellite imagery. In *Proceedings of the 26th ACM SIGKDD International Conference on Knowledge Discovery & Data Mining*, pages 2970–2979, 2020.
- [22] Kaiming He, Xiangyu Zhang, Shaoqing Ren, and Jian Sun. Deep residual learning for image recognition. In *Proceedings of the IEEE conference on computer vision and pattern recognition*, pages 770–778, 2016.
- [23] Kaiming He, Xinlei Chen, Saining Xie, Yanghao Li, Piotr Dollár, and Ross Girshick. Masked autoencoders are scalable vision learners. In *Proceedings of the IEEE/CVF conference on computer vision and pattern recognition*, pages 16000–16009, 2022.
- [24] Zhiyuan He, Su Yang, Weishan Zhang, and Jiulong Zhang. Perceiving commercial activeness over satellite images. In *Companion Proceedings of the The Web Conference 2018*, pages 387–394, 2018.
- [25] Jack Hessel, Ari Holtzman, Maxwell Forbes, Ronan Le Bras, and Yejin Choi. CLIPScore: A reference-free evaluation metric for image captioning. In Marie-Francine Moens, Xuanjing Huang, Lucia Specia, and Scott Wen-tau Yih, editors, *Proceedings of the 2021 Conference on Empirical Methods in Natural Language Processing*, pages 7514–7528, Online and Punta Cana, Dominican Republic, November 2021. Association for Computational Linguistics. doi: 10.18653/v1/2021.emnlp-main.595. URL <https://aclanthology.org/2021.emnlp-main.595>.

- [26] Anwen Hu, Shizhe Chen, Liang Zhang, and Qin Jin. Infometric: An informative metric for reference-free image caption evaluation. *arXiv preprint arXiv:2305.06002*, 2023.
- [27] Yingjing Huang, Fan Zhang, Yong Gao, Wei Tu, Fabio Duarte, Carlo Ratti, Diansheng Guo, and Yu Liu. Comprehensive urban space representation with varying numbers of street-level images. *Computers, Environment and Urban Systems*, 106:102043, 2023. ISSN 0198-9715. doi: <https://doi.org/10.1016/j.compenvurbsys.2023.102043>. URL <https://www.sciencedirect.com/science/article/pii/S0198971523001060>.
- [28] Ashish Jaiswal, Ashwin Ramesh Babu, Mohammad Zaki Zadeh, Debapriya Banerjee, and Fillia Makedon. A survey on contrastive self-supervised learning. *Technologies*, 9(1):2, 2020.
- [29] Porter Jenkins, Ahmad Farag, Suhang Wang, and Zhenhui Li. Unsupervised representation learning of spatial data via multimodal embedding. In *Proceedings of the 28th ACM International Conference on Information and Knowledge Management, CIKM '19*, page 1993–2002, New York, NY, USA, 2019. Association for Computing Machinery. ISBN 9781450369763. doi: 10.1145/3357384.3358001. URL <https://doi.org/10.1145/3357384.3358001>.
- [30] Chao Jia, Yinfei Yang, Ye Xia, Yi-Ting Chen, Zarana Parekh, Hieu Pham, Quoc Le, Yun-Hsuan Sung, Zhen Li, and Tom Duerig. Scaling up visual and vision-language representation learning with noisy text supervision. In *International conference on machine learning*, pages 4904–4916. PMLR, 2021.
- [31] Wonjae Kim, Bokyoung Son, and Ildoo Kim. Vilt: Vision-and-language transformer without convolution or region supervision. In *International Conference on Machine Learning*, pages 5583–5594. PMLR, 2021.
- [32] Zhengfeng Lai, Haotian Zhang, Wentao Wu, Haoping Bai, Aleksei Timofeev, Xianzhi Du, Zhe Gan, Jiulong Shan, Chen-Nee Chuah, Yinfei Yang, et al. From scarcity to efficiency: Improving clip training via visual-enriched captions. *arXiv preprint arXiv:2310.07699*, 2023.
- [33] Stephen Law, Brooks Paige, and Chris Russell. Take a look around: Using street view and satellite images to estimate house prices. *ACM Trans. Intell. Syst. Technol.*, 10(5), sep 2019. ISSN 2157-6904. doi: 10.1145/3342240. URL <https://doi.org/10.1145/3342240>.
- [34] Hwanhee Lee, Seunghyun Yoon, Franck Dernoncourt, Doo Soon Kim, Trung Bui, and Kyomin Jung. Viltbertscore: Evaluating image caption using vision-and-language bert. In *Proceedings of the First Workshop on Evaluation and Comparison of NLP Systems*, pages 34–39, 2020.
- [35] Gen Li, Nan Duan, Yuejian Fang, Ming Gong, and Daxin Jiang. Unicoder-vl: A universal encoder for vision and language by cross-modal pre-training. In *Proceedings of the AAAI conference on artificial intelligence*, volume 34, pages 11336–11344, 2020.
- [36] Junnan Li, Dongxu Li, Caiming Xiong, and Steven Hoi. Blip: Bootstrapping language-image pre-training for unified vision-language understanding and generation. In *International Conference on Machine Learning*, pages 12888–12900. PMLR, 2022.
- [37] Junnan Li, Dongxu Li, Silvio Savarese, and Steven Hoi. Blip-2: Bootstrapping language-image pre-training with frozen image encoders and large language models. *arXiv preprint arXiv:2301.12597*, 2023.
- [38] Liunian Harold Li, Pengchuan Zhang, Haotian Zhang, Jianwei Yang, Chunyuan Li, Yiwu Zhong, Lijuan Wang, Lu Yuan, Lei Zhang, Jenq-Neng Hwang, et al. Grounded language-image pre-training. In *Proceedings of the IEEE/CVF Conference on Computer Vision and Pattern Recognition*, pages 10965–10975, 2022.
- [39] Shuzhe Li, Wei Chen, Bingqi Yan, Zhen Li, Shunzhi Zhu, and Yanwei Yu. Self-supervised contrastive representation learning for large-scale trajectories. *Future Generation Computer Systems*, 2023.
- [40] Shuzhe Li, Wei Chen, Bin Wang, Chao Huang, Yanwei Yu, and Junyu Dong. Mcn4rec: Multi-level collaborative neural network for next location recommendation. *ACM Trans. Inf. Syst.*, 42(4), mar 2024. ISSN 1046-8188. doi: 10.1145/3643669. URL <https://doi.org/10.1145/3643669>.

- [41] Tong Li, Shiduo Xin, Yanxin Xi, Sasu Tarkoma, Pan Hui, and Yong Li. Predicting multi-level socioeconomic indicators from structural urban imagery. In *Proceedings of the 31st ACM International Conference on Information & Knowledge Management, CIKM '22*, page 3282–3291, New York, NY, USA, 2022. Association for Computing Machinery. ISBN 9781450392365. doi: 10.1145/3511808.3557153. URL <https://doi.org/10.1145/3511808.3557153>.
- [42] Tong Li, Shiduo Xin, Yanxin Xi, Sasu Tarkoma, Pan Hui, and Yong Li. Predicting multi-level socioeconomic indicators from structural urban imagery. In *Proceedings of the 31st ACM International Conference on Information & Knowledge Management*, pages 3282–3291, 2022.
- [43] Yangguang Li, Feng Liang, Lichen Zhao, Yufeng Cui, Wanli Ouyang, Jing Shao, Fengwei Yu, and Junjie Yan. Supervision exists everywhere: A data efficient contrastive language-image pre-training paradigm. *arXiv preprint arXiv:2110.05208*, 2021.
- [44] Zechen Li, Weiming Huang, Kai Zhao, Min Yang, Yongshun Gong, and Meng Chen. Urban region embedding via multi-view contrastive prediction. *arXiv preprint arXiv:2312.09681*, 2023.
- [45] Yunlei Liang, Jiawei Zhu, Wen Ye, and Song Gao. Region2vec: Community detection on spatial networks using graph embedding with node attributes and spatial interactions. In *Proceedings of the 30th International Conference on Advances in Geographic Information Systems*, pages 1–4, 2022.
- [46] Yuxuan Liang, Songyu Ke, Junbo Zhang, Xiuwen Yi, and Yu Zheng. Geoman: Multi-level attention networks for geo-sensory time series prediction. In *IJCAI*, volume 2018, pages 3428–3434, 2018.
- [47] Yuxuan Liang, Kun Ouyang, Junkai Sun, Yiwei Wang, Junbo Zhang, Yu Zheng, David Rosenblum, and Roger Zimmermann. Fine-grained urban flow prediction. In *Proceedings of the Web Conference 2021*, pages 1833–1845, 2021.
- [48] Haotian Liu, Chunyuan Li, Yuheng Li, and Yong Jae Lee. Improved baselines with visual instruction tuning. *arXiv preprint arXiv:2310.03744*, 2023.
- [49] Haotian Liu, Chunyuan Li, Qingyang Wu, and Yong Jae Lee. Visual instruction tuning. *arXiv preprint arXiv:2304.08485*, 2023.
- [50] Shilong Liu, Zhaoyang Zeng, Tianhe Ren, Feng Li, Hao Zhang, Jie Yang, Chunyuan Li, Jianwei Yang, Hang Su, Jun Zhu, et al. Grounding dino: Marrying dino with grounded pre-training for open-set object detection. *arXiv preprint arXiv:2303.05499*, 2023.
- [51] Yu Liu, Xin Zhang, Jingtao Ding, Yanxin Xi, and Yong Li. Knowledge-infused contrastive learning for urban imagery-based socioeconomic prediction. In *Proceedings of the ACM Web Conference 2023*, pages 4150–4160, 2023.
- [52] Jiasen Lu, Dhruv Batra, Devi Parikh, and Stefan Lee. *ViLBERT: pretraining task-agnostic visiolinguistic representations for vision-and-language tasks*. Curran Associates Inc., Red Hook, NY, USA, 2019.
- [53] Rose M Rustowicz, Robin Cheong, Lijing Wang, Stefano Ermon, Marshall Burke, and David Lobell. Semantic segmentation of crop type in africa: A novel dataset and analysis of deep learning methods. In *Proceedings of the IEEE/CVF Conference on Computer Vision and Pattern Recognition Workshops*, pages 75–82, 2019.
- [54] Gengchen Mai, Krzysztof Janowicz, Yingjie Hu, Song Gao, Bo Yan, Rui Zhu, Ling Cai, and Ni Lao. A review of location encoding for geoai: methods and applications. *International Journal of Geographical Information Science*, 36(4):639–673, 2022.
- [55] Rohin Manvi, Samar Khanna, Gengchen Mai, Marshall Burke, David Lobell, and Stefano Ermon. Geollm: Extracting geospatial knowledge from large language models. *arXiv preprint arXiv:2310.06213*, 2023.
- [56] Mapbox. Mapbox - Location Data & Maps for Developers. URL <https://www.mapbox.com/>.

- [57] Jorge Andres Chamorro Martinez, Laura Elena Cué La Rosa, Raul Queiroz Feitosa, Ieda Del’ Arco Sanches, and Patrick Nigri Happ. Fully convolutional recurrent networks for multivariate crop recognition from multitemporal image sequences. *ISPRS Journal of Photogrammetry and Remote Sensing*, 171:188–201, 2021.
- [58] Long Ouyang, Jeffrey Wu, Xu Jiang, Diogo Almeida, Carroll Wainwright, Pamela Mishkin, Chong Zhang, Sandhini Agarwal, Katarina Slama, Alex Ray, et al. Training language models to follow instructions with human feedback. *Advances in Neural Information Processing Systems*, 35:27730–27744, 2022.
- [59] Anthony Perez, Christopher Yeh, George Azzari, Marshall Burke, David Lobell, and Stefano Ermon. Poverty prediction with public landsat 7 satellite imagery and machine learning. *arXiv preprint arXiv:1711.03654*, 2017.
- [60] Dustin Podell, Zion English, Kyle Lacey, Andreas Blattmann, Tim Dockhorn, Jonas Müller, Joe Penna, and Robin Rombach. Sdxl: Improving latent diffusion models for high-resolution image synthesis. *arXiv preprint arXiv:2307.01952*, 2023.
- [61] Alec Radford, Jong Wook Kim, Chris Hallacy, Aditya Ramesh, Gabriel Goh, Sandhini Agarwal, Girish Sastry, Amanda Askell, Pamela Mishkin, Jack Clark, et al. Learning transferable visual models from natural language supervision. In *International conference on machine learning*, pages 8748–8763. PMLR, 2021.
- [62] Vipula Rawte, Amit Sheth, and Amitava Das. A survey of hallucination in large foundation models. *arXiv preprint arXiv:2309.05922*, 2023.
- [63] Marc Rußwurm and Marco Körner. Self-attention for raw optical satellite time series classification. *ISPRS journal of photogrammetry and remote sensing*, 169:421–435, 2020.
- [64] Gwanghwan Seong, Namwoo Kim, Seyun Kim, and Yoonjin Yoon. Multi-modal based region representation learning considering mobility data in seoul. *Procedia Computer Science*, 220: 251–258, 2023. ISSN 1877-0509. doi: <https://doi.org/10.1016/j.procs.2023.03.153>. URL <https://www.sciencedirect.com/science/article/pii/S1877050923006889>. The 14th International Conference on Ambient Systems, Networks and Technologies Networks (ANT) and The 6th International Conference on Emerging Data and Industry 4.0 (EDI40).
- [65] Naeha Sharif, Lyndon White, Mohammed Bennamoun, and Syed Afaq Ali Shah. Nneval: Neural network based evaluation metric for image captioning. In *Proceedings of the European Conference on Computer Vision (ECCV)*, pages 37–53, 2018.
- [66] Hao Hao Tan and Mohit Bansal. Lxmert: Learning cross-modality encoder representations from transformers. In *Conference on Empirical Methods in Natural Language Processing*, 2019. URL <https://api.semanticscholar.org/CorpusID:201103729>.
- [67] Maria Tsimpoukelli, Jacob L Menick, Serkan Cabi, SM Eslami, Oriol Vinyals, and Felix Hill. Multimodal few-shot learning with frozen language models. *Advances in Neural Information Processing Systems*, 34:200–212, 2021.
- [68] Ashish Vaswani, Noam Shazeer, Niki Parmar, Jakob Uszkoreit, Llion Jones, Aidan N Gomez, Łukasz Kaiser, and Illia Polosukhin. Attention is all you need. *Advances in neural information processing systems*, 30, 2017.
- [69] Vicente Vivanco, Gaurav Kumar Nayak, and Mubarak Shah. Geoclip: Clip-inspired alignment between locations and images for effective worldwide geo-localization. 2023.
- [70] Anna X Wang, Caelin Tran, Nikhil Desai, David Lobell, and Stefano Ermon. Deep transfer learning for crop yield prediction with remote sensing data. In *Proceedings of the 1st ACM SIGCAS Conference on Computing and Sustainable Societies*, pages 1–5, 2018.
- [71] Hongjian Wang and Zhenhui Li. Region representation learning via mobility flow. In *Proceedings of the 2017 ACM on Conference on Information and Knowledge Management, CIKM ’17*, page 237–246, New York, NY, USA, 2017. Association for Computing Machinery. ISBN 9781450349185. doi: 10.1145/3132847.3133006. URL <https://doi.org/10.1145/3132847.3133006>.

- [72] Zhecheng Wang, Haoyuan Li, and Ram Rajagopal. Urban2vec: Incorporating street view imagery and pois for multi-modal urban neighborhood embedding. In *Proceedings of the AAAI Conference on Artificial Intelligence*, volume 34, pages 1013–1020, 2020.
- [73] Yanxin Xi, Tong Li, Huandong Wang, Yong Li, Sasu Tarkoma, and Pan Hui. Beyond the first law of geography: Learning representations of satellite imagery by leveraging point-of-interests. In *Proceedings of the ACM Web Conference 2022*, pages 3308–3316, 2022.
- [74] Yibo Yan, Haomin Wen, Siru Zhong, Wei Chen, Haodong Chen, Qingsong Wen, Roger Zimmermann, and Yuxuan Liang. Urbanclip: Learning text-enhanced urban region profiling with contrastive language-image pretraining from the web. In *Proceedings of the ACM on Web Conference 2024, WWW '24*, page 4006–4017, New York, NY, USA, 2024. Association for Computing Machinery. ISBN 9798400701719. doi: 10.1145/3589334.3645378. URL <https://doi.org/10.1145/3589334.3645378>.
- [75] Zhengyuan Yang, Linjie Li, Kevin Lin, Jianfeng Wang, Chung-Ching Lin, Zicheng Liu, and Lijuan Wang. The dawn of Imms: Preliminary explorations with gpt-4v (ision). *arXiv preprint arXiv:2309.17421*, 9(1), 2023.
- [76] Lewei Yao, Runhui Huang, Lu Hou, Guansong Lu, Minzhe Niu, Hang Xu, Xiaodan Liang, Zhenguo Li, Xin Jiang, and Chunjing Xu. FILIP: Fine-grained interactive language-image pre-training. In *International Conference on Learning Representations*, 2022. URL <https://openreview.net/forum?id=cpDhcsEDC2>.
- [77] Qinghao Ye, Haiyang Xu, Guohai Xu, Jiabo Ye, Ming Yan, Yiyang Zhou, Junyang Wang, Anwen Hu, Pengcheng Shi, Yaya Shi, et al. mplug-owl: Modularization empowers large language models with multimodality. *arXiv preprint arXiv:2304.14178*, 2023.
- [78] Christopher Yeh, Chenlin Meng, Sherrie Wang, Anne Driscoll, Erik Rozi, Patrick Liu, Ji-hyeon Lee, Marshall Burke, David B Lobell, and Stefano Ermon. Sustainbench: Benchmarks for monitoring the sustainable development goals with machine learning. *arXiv preprint arXiv:2111.04724*, 2021.
- [79] Yifang Yin, Ying Zhang, Zhenguang Liu, Yuxuan Liang, Sheng Wang, Rajiv Ratn Shah, and Roger Zimmermann. Learning multi-context aware location representations from large-scale geotagged images. In *Proceedings of the 29th ACM International Conference on Multimedia, MM '21*, page 899–907, New York, NY, USA, 2021. Association for Computing Machinery. ISBN 9781450386517. doi: 10.1145/3474085.3475268. URL <https://doi.org/10.1145/3474085.3475268>.
- [80] Jiakuan You, Xiaocheng Li, Melvin Low, David Lobell, and Stefano Ermon. Deep gaussian process for crop yield prediction based on remote sensing data. In *Proceedings of the AAAI conference on artificial intelligence*, volume 31, 2017.
- [81] Haotian Zhang, Pengchuan Zhang, Xiaowei Hu, Yen-Chun Chen, Liunian Li, Xiyang Dai, Lijuan Wang, Lu Yuan, Jenq-Neng Hwang, and Jianfeng Gao. Glipv2: Unifying localization and vision-language understanding. *Advances in Neural Information Processing Systems*, 35: 36067–36080, 2022.
- [82] Mingyang Zhang, Tong Li, Yong Li, and Pan Hui. Multi-view joint graph representation learning for urban region embedding. In *Proceedings of the Twenty-Ninth International Conference on International Joint Conferences on Artificial Intelligence*, pages 4431–4437, 2021.
- [83] Tianyi Zhang, Varsha Kishore, Felix Wu, Kilian Q. Weinberger, and Yoav Artzi. Bertscore: Evaluating text generation with BERT. In *8th International Conference on Learning Representations, ICLR 2020, Addis Ababa, Ethiopia, April 26-30, 2020*. OpenReview.net, 2020. URL <https://openreview.net/forum?id=SkeHuCVFDr>.
- [84] Wayne Xin Zhao, Kun Zhou, Junyi Li, Tianyi Tang, Xiaolei Wang, Yupeng Hou, Yingqian Min, Beichen Zhang, Junjie Zhang, Zican Dong, et al. A survey of large language models. *arXiv preprint arXiv:2303.18223*, 2023.

- [85] Yu Zheng, Licia Capra, Ouri Wolfson, and Hai Yang. Urban computing: concepts, methodologies, and applications. *ACM Transactions on Intelligent Systems and Technology (TIST)*, 5(3): 1–55, 2014.
- [86] Siru Zhong, Xixuan Hao, Yibo Yan, Ying Zhang, Yangqiu Song, and Yuxuan Liang. Urban-cross: Enhancing satellite image-text retrieval with cross-domain adaptation. *arXiv preprint arXiv:2404.14241*, 2024.
- [87] X Zhong, Q Yan, and G Li. Long time series nighttime light dataset of china (2000–2020). *Digit. J. Glob. Change Data Repos*, 6, 2022.
- [88] Xingchen Zou, Yibo Yan, Xixuan Hao, Yuehong Hu, Haomin Wen, Erdong Liu, Junbo Zhang, Yong Li, Tianrui Li, Yu Zheng, et al. Deep learning for cross-domain data fusion in urban computing: Taxonomy, advances, and outlook. *arXiv preprint arXiv:2402.19348*, 2024.

Appendix / supplemental material

A Formulation

Definition 1 (Urban Region) We follow previous research [73, 74] and *evenly* divide the target area (*e.g.* a city) into L urban regions.

Definition 2 (Urban Imagery) Diverse visual images, including satellite and street-view images, facilitate an intuitive analysis of urban regions. Specifically, *satellite images* provide a coarse-grained overview of the structural composition of a region. Each input satellite image *w.r.t* the urban area g can be represented as $I_g^{sa} \in \mathbb{R}^{H \times W \times 3}$, where H and W denote the length and width. *Street-view images* are captured by vehicles from map providers during urban traversals, offering detailed visual information on the fine-grained aspects within a region. By querying the latitude and longitude range of satellite images, multiple street-view images are associated together *w.r.t* the urban region g based on their locations \mathcal{L}_g . Each individual street-view image is represented as $I_g^{sv} \in \mathbb{R}^{H \times W \times 3}$.

Definition 3 (Text Description) Textual descriptions of urban area g (including satellite text T_g^{sa} and street-view text T_g^{sv}) provide precise means for urban area analysis. Such text can be manually generated or produced using image annotation tools. Particularly, leveraging advanced LLMs enables detailed and insightful analytical descriptions of given area images. Notably, incorporating spatial context (*e.g.* vegetation coverage and POI) significantly reflects the functional characteristics of the region.

Definition 4 (Urban Indicators) Urban indicators assess various aspects of a region, including population, economy, society, and public services, from multiple perspectives. A set of L urban regions with K indicators is represented as $\mathbf{Y} \in \mathbb{R}^{L \times K}$. In this paper, we comprehensively use *population* (count), *GDP* (in million Chinese Yuan), *carbon emissions* (in tons), *night lights* (intensity), *house prices* (in Chinese Yuan), and *points of interest*, *i.e.* *POI*, (count for different categories) as ground-truth urban indicators.

B More Details about Datasets & Tasks

B.1 CityScape Dataset

We construct the CityScape Dataset using street-view geo-tagged images collected from Baidu Map API and generated text descriptions by LMM.

- **Street-View Panoramic Image Collection.** The Street-View image sampling process utilized the Baidu Maps API², facilitating the extraction of road network data within our predefined sampling area. Using the ArcGIS³ tool, we exported the road network data and established a sampling interval of 500 meters, which allowed for the comprehensive collection of street-view images at every half-kilometer point along the road network, ensuring thorough coverage that complements the satellite imagery’s scope. Following the road network sampling, panoramic street-view images were collected based on the sampling points. These images, with a resolution of 2048x664, also far exceed the 256x256 resolution of satellite imagery [74], ensuring clarity and ample details for further analysis.

As is shown in Table 2, a total of 47,582 street-level images were collected, whose data volume is 2.7 times larger than that of the satellite dataset, capturing the intricacies of the urban landscape and providing a street-level view that enhances the overall urban analysis.

In figure 11, we showcase our sampling process for the road network, which is used to collect street-view imagery at strategically selected locations. We initially acquire road network data from the online open-source website and subsequently import it into ArcGIS with a sampling interval of 500 meters. Following this, we gather the latitude and longitude coordinates of the sampling points within our dataset area. These coordinates are then used to invoke the Baidu API to collect street-view imagery. Additionally, not all sampled points have corresponding street view images, thereby resulting in a final count of street view images that is less than the number of sampled points.

²<https://lbsyun.baidu.com/>

³<https://www.esri.com/en-us/arcgis/products/develop-with-arcgis/overview>

- **Corresponding Text Description Generation.** The textual data corresponding to each street-view image is generated from ShareGPT4V [11], which is recognized for its superior text generation capabilities compared to other contemporary open-source LMM models [48, 14, 77, 20, 10, 11], offering comprehensive and high-quality textual information. The quality of the generated data is guaranteed by our proposed PerceptionScore. We filter out the texts with PerceptionScore lower than 0.5.

Table 2: Urban imagery dataset statistics.

Dataset	Coverage		#Street -view Image	#Satellite Image
	Bottom-left	Top-right		
Beijing	39.75°N, 116.03°E	40.15°N, 116.79°E	14,164	4,592
Shanghai	30.98°N, 121.10°E	31.51°N, 121.80°E	15,616	5,244
Guangzhou	22.94°N, 113.10°E	23.40°N, 113.68°E	7,635	3,402
Shenzhen	22.45°N, 113.75°E	22.84°N, 114.62°E	10,167	4,324

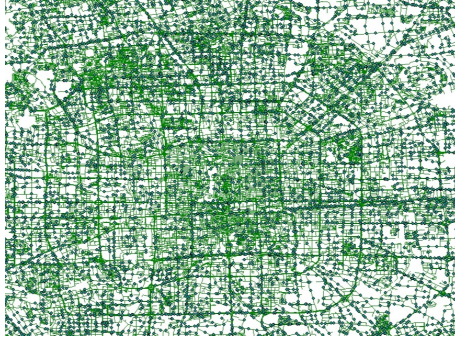


Figure 11: Road Network Sampling for Street-View Images on Beijing.

B.2 Downstream Dataset & Tasks

In our research, the Downstream Dataset plays a crucial role in gauging the practical implications of our multimodal framework. We collect six representative urban indicators: *Carbon Emission*, *Population*, *GDP*, *Night Light*, *House Price*, and *POI*. Each indicator illuminates a significant dimension of urban vitality and sustainability. In this section, we provide the detailed introduction and data source of our downstream benchmark.

- **Carbon Emissions:** Extracted from the Open-source Data Inventory for Anthropogenic CO₂ (ODIAC), this dataset offers granular carbon emission figures in 2022 that are in alignment with the spatial resolution of our satellite imagery, which is one square kilometer per image. The emissions are quantified in tons.
- **Population:** The quantum of population serves as an indicator of a region’s sociodemographic characteristics. Sourced from WorldPop (<https://hub.worldpop.org>), we gather population distribution data in 2020, to provide an in-depth portrayal of demographic patterns. The unit is #citizens.
- **GDP:** This dataset encapsulates China’s economic development by incorporating Gross Domestic Product (GDP) figures, thereby infusing an economic dimension into our analysis of urban regions. The unit is million Chinese Yuan.
- **Night Light:** Nighttime light can, to some extent, characterize the intensity of human activities, which is of great significance for urban development studies. we take the nightlight data from [87] in 2020.
- **House Price:** The price of housing is subject to the influence of numerous socio-economic factors. By observing fluctuations in housing prices, it is possible to discern, to a certain extent, the state of economic development. We collect data from Anjuke (<https://www.anjuke.com>) in March 2023 with yuan/m² unit. Individual house price represents a locational attribute. To extrapolate a regional-level characteristic, we take the average of housing prices across an urban region.

- **POI:** The spatial distribution of various types of POIs (Points of Interest) within urban areas is a potent social indicator, as it reflects the underlying social and economic architecture, as well as the population’s activities and urban lifestyles. Consequently, to glean insights into these urban dynamics, we collect data of POIs from web sources, encompassing both their locations and categories. The collected data has 14 categories: *Dining and Cuisine, Leisure and Entertainment, Sports and Fitness, Business and Residential, Healthcare, Financial Institutions, Tourist Attractions, Lifestyle Services, Shopping and Consumption, Automobile Related, Hotel Accommodation, Transport Facilities, Science, Education and Culture, Companies and Enterprises*. To capture the unique attributes of each area, we aggregate the number of POIs by category within each region.

We construct this benchmark with the aim of conducting a thorough evaluation of the urban region representations that have been derived through our learning framework. We uniformly partition the downstream dataset into train:val:test=7:1:2. These indicators constitute the downstream task dataset, covering economic (GDP, Night Light, House Price), social (Population, POI), and environmental (Carbon Emission) indicators. The data preprocessing setting adheres to [74] with refinement. For some indicators data with relatively small differences in values, we have taken the logarithm of these values to facilitate training.

B.3 Downstream Dataset Analysis

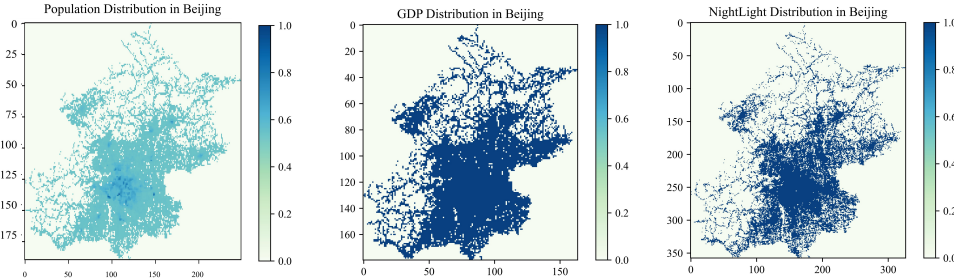


Figure 12: Spatial distribution of Population, GDP and NightLight in Beijing.

Here we visualize the distribution of some downstream socio-economic indicator data on Beijing in Figure 12. The distribution of different indicators exhibits similar trends, indicating that Beijing has a clear ‘center-periphery’ structure, with the core area being densely populated and economically developed, while the peripheral areas are relatively sparse.

Beyond geographical spatial differences, the concentration trends and variability of the data are critical perspectives that merit attention. In Figure 13 we demonstrate these patterns by illustrating the normalized values of different socio-economic indicators in Beijing. Outliers with extreme maximum and minimum values will be filtered out during our processing. As we can see, the values of Carbon Emission and NightLight are relatively concentrated, showing minimal variability. The distribution of GDP values is more widespread, while Population distribution exhibits a bimodal characteristic, reflecting the inherent diversity.

C In-depth Overview of Baseline Methods

The single granularity imagery-based urban region representation learning methods include:

- **ViT [15]:** ViT is a successful paradigm of applying transformers to computer vision, where images are segmented into patches for fixed-length modeling. When sufficient data is available for pre-training, ViT’s performance can surpass that of CNNs [22]. In our experiment, we leverage ViT-B as the baseline for comparison.
- **PG-SimCLR [73]:** A contrastive learning framework which introduces geographic information (i.e., POI) into urban region representation learning. In our study, we do not employ PG-SimCLR to predict POI to ensure a fair comparison.

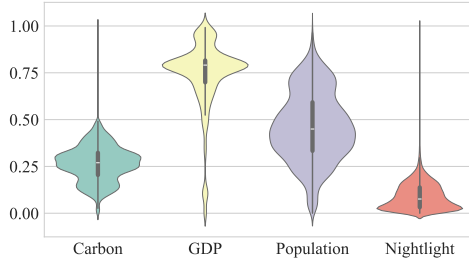


Figure 13: Data distribution of Carbon Emission, Population, GDP and NightLight in Beijing.

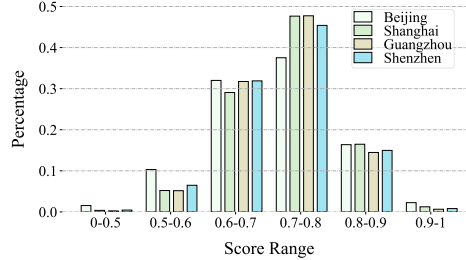


Figure 14: PerceptionScore distribution on CityScape dataset for 4 representative cities.

- **UrbanCLIP [74]:** A model that utilizes an image-text contrastive learning-based approach for learning robust representations from urban imagery, intending to capture the complexity and diversity of urban areas.
- **UrbanCLIP-SV [74]:** Original UrbanCLIP is pretrained on satellite image-text pairs. Here we also verify its performance on our proposed CityScape dataset, utilizing the same aggregation method to acquire regional features.

We also apply multiple baselines for multi-granularity urban imagery-based representation learning:

- **Vision-LSTM [27]:** A vision long short-term memory neural network which could process variable-length street-view image within each region. The integration of satellite and street-view imagery, along with trajectories, facilitates a more effective capture of comprehensive urban representations, yielding reliable recognition results.
- **StructuralUrban[41]:** The graph-based framework for urban region profiling leveraging street segments as containers to adaptively fuse the features of multi-level urban images. We term this method StructuralUrban for simplicity.

We present a visual representation of the performance in the main paper Figure 4 to effectively demonstrate the comprehensive capabilities of our model across various downstream tasks. There is also a trend that models tend to perform better on environmental (Carbon Emission) and social (Population, POI) indicators than on economic (GDP, Night Light, House Price) indicators. This is possibly because environmental and social indicators usually have more distinct geographic distribution characteristics. For instance, neighboring regions may have similar climates, vegetation cover, and population densities, which are important factors for environmental and social indicators and can be effectively captured through spatial embedding. On the other hand, economic indicators are more complex and influenced by various factors, including policies, economic activities, and market sentiments, making them harder to model. Additionally, due to the multi-class nature of POI, models may require more complex structures to understand the underlying relationships between labels, thus resulting in lower performance.

D Implementation Details

In our experiment, Adam optimizer is chosen to minimize the training loss during parameter learning. A grid search on hyperparameters is conducted, where search ranges for learning rate and batch size are set as $2e-6$, $2e-5$, $2e-4$, $2e-3$, $2e-2$ and 4, 8, 16, 32, 64, respectively. The data augmentation strategy follows the setting of [61]. The weight hyperparameter α and β of \mathcal{L}_{Total} are set to 0.5, 0.5 respectively. We run all the models on NVIDIA A800 GPUs with PyTorch.

We implement the aggregation method $\text{Aggr}(\cdot)$ through MLP layers. The feature fusion method f directly utilizes additive aggregation. To ensure a fixed length for network processing, we set the maximum street-view sequence length within one region as 25, and sequences shorter than that are achieved by padding with zeros. For the semantic segmentation model to decouple visual elements with street-view images, following [17], the architecture for the semantic model is *ResNet18dilated* + *PPM_deepsup*. Initially, the dataset comprises 150 segmentation categories. However, in line with

our requirements, we narrow down the selection to 38 categories, which we further group into 13 street-view features following [17]: *Person; Bike; Heavy Vehicle; Light Vehicle; Facade; Window & Opening; Road; Sidewalk; Street Furniture; Greenery - Tree; Greenery - Grass & Shrubs; Sky; Nature.*

E More Details for Modality Representation

For utilizing ViT as the visual encoder to process urban visual data, in particular, we reshape the input image $I \in \mathbb{R}^{H \times W \times 3}$ into a sequence of flattened 2D patches $I_P \in \mathbb{R}^{N \times (P^2 \cdot C)}$, where C represents the number of channels, (P, P) specifies the resolution of each image patch, and $N = HW/P^2$ denotes the number of patches, corresponding to the input sequence length for ViT. Notably, the ViT utilizes a consistent latent vector size (denoted as d) across all its layers. Thus, we can obtain the outputs as the patch embeddings through a trainable linear projection. We also prepend a learnable embedding to the patch embedding sequence (i.e., $\mathbf{z}_0^0 = I_{cls}$). Besides, we add learnable position embedding \mathbf{E}_{pos} to retain positional information. The process is as follows:

$$\mathbf{z}_0 = [I_{cls}; I_P^1 \mathbf{W}; I_P^2 \mathbf{W}; \dots; I_P^N \mathbf{W}] + \mathbf{E}_{pos}, \quad (8)$$

where $\mathbf{W} \in \mathbb{R}^{(P^2 \cdot C) \times d}$ and $\mathbf{E}_{pos} \in \mathbb{R}^{(N+1) \times d}$ are learnable parameters. \mathbf{z}_0 represents the result of the linear projection, which is subsequently fed into the ViT.

Consistent with the standard Transformer encoder, ViT includes alternating layers of multi-head self-attention $\text{MSA}(\cdot)$ operation [68]. Furthermore, layer normalization (LN) is adopted before every block, whereas residual connections are after every block:

$$\mathbf{z}_l = \text{MSA}(\text{LN}(\mathbf{z}_{l-1})) + \mathbf{z}_{l-1}, \quad l = 1 \dots L. \quad (9)$$

The text encoder follows a similar MSA mechanism of the visual encoder. The input text sequence is bracketed with $[SOS]$ and $[EOS]$ tokens, and the activation of the highest layer of Transformer at $[EOS]$ token is considered the global representation \mathbf{z}_T of text.

F Segmentation Ratio and Prompt Examples

As illustrated in Figure 15(a) and (b), we demonstrate examples of the segmentation ratio of street-view images in our CityScape dataset. The segmentation ratio is decoupled by pretrained segmentation models and is used in both prompt construction and PerceptionScore computation. We group the segmentation categories into 13 categories following [17]: *Person; Bike; Heavy Vehicle; Light Vehicle; Facade; Window & Opening; Road; Sidewalk; Street Furniture; Greenery - Tree; Greenery - Grass & Shrubs; Sky; Nature.*

The prompt template used to generate street-view descriptions is formulated as follows: *Analyze the street-view panoramic image in [City] in a comprehensive and detailed manner. The coordinate of the street-view image is [Longitude, Latitude]. The segmentation ratio of the street-view image is [Segment Information].* Figure 15(c) provides illustrations of some examples of our prompts used for description generation.

G The Choice of Image-to-Text LMM

In our work, we leverage ShareGPT4V [11] for text description generation. Here we conduct experiments on current open-sourced LMM models, and compute the PerceptionScore of them. The results are presented in Table 3. As we can see, ShareGPT4V achieves the best performance in terms of PerceptionScore, followed by LLaMA-Adapter V2, which is used as the Image-to-Text models in [74]. Additionally, we note that there is study [86] argue that InstructBLIP [14] exhibits state-of-the-art (SOTA) performance in image-to-text generation. However, in our experiment, we found that InstructBLIP is unsuitable for handling geospatial coordinates as prompt content. Incorporating such coordinates significantly degrades the quality of the generated text, leading to poor content output. Due to these limitations, we have excluded it from our comparative analysis.

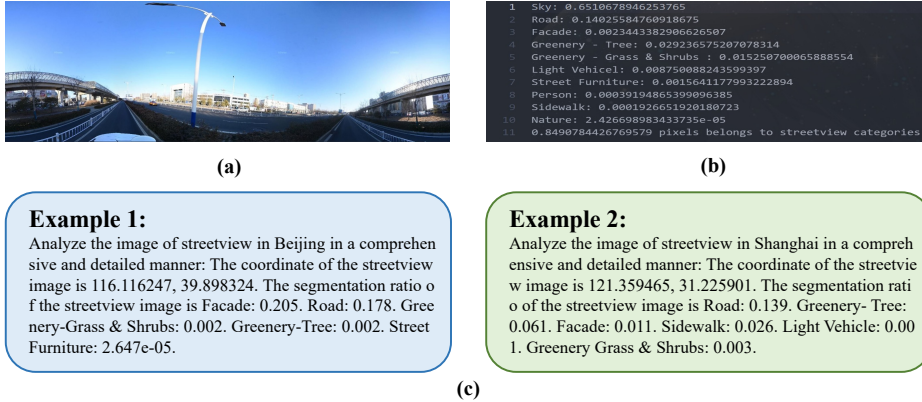


Figure 15: Prompt Examples.

Table 3: Perception score of representative LMMs.

Models	Average Generated-Description Scores
LLaVA-v1.5 [48]	0.674
mPLUG-Owl [77]	0.662
LLaMA-Adapter V2 [20]	0.698
MiniGPTv2 [10]	0.693
ShareGPT4V [11]	0.714

H More Experimental Analysis

H.1 More Analysis for Text Calibration

In our paper, we selected the state-of-the-art LMM ShareGPT4V, which demonstrates performance comparable to GPT4V in image captioning. In order to ascertain the efficacy of ShareGPT4V, we computed the distribution of PerceptionScore for descriptions generated by ShareGPT4V, as depicted in Figure 14. Notably, only less than 0.02% of generated texts scored below 0.5, thereby evidencing the high quality of the descriptions produced.

As a result, the experimental results comparing with and without calibration do not adequately reflect the effectiveness of our calibration method. To further demonstrate the effectiveness of our method, we select mPLUG-Owl [77], one of the representative LMMs compared in our paper, with the worst performance. After calibration, 15.3% of the text with perceptionscores below 0.5 was filtered out. The results validate the effectiveness of our calibration method, and indicate that more relevant and noise-free textual information could align better with image features, leading to a more coherent and meaningful visual representation.

Table 4: UrbanVLP performance utilizing mPLUG-Owl with and without Text Calibration. mPO is an abbreviation for mPLUG-Owl, and TC stands for Text Calibration.

Model	Carbon			Population			GDP		
	R ²	RMSE	MAE	R ²	RMSE	MAE	R ²	RMSE	MAE
UrbanVLP_mPO_wo TC	0.687	0.551	0.544	0.643	0.580	0.458	0.494	0.655	0.447
UrbanVLP_mPO	0.714	0.538	0.473	0.683	0.557	0.430	0.506	0.640	0.435
UrbanVLP	0.769	0.477	0.369	0.714	0.523	0.411	0.537	0.684	0.416

H.2 Analysis about Time Complexity

Modeling and research in urban areas can provide valuable references and assistance to policymakers, builders, and citizens. Therefore, practical implementation should be considered. We conduct time complexity analysis using FPS (Frames Per Second), a common indicator for inference speed in computer vision area. We report FPS for satellite image in Figure 16(b). In fact, introducing street view features for better and finer-grained effects will inevitably sacrifice a portion of the time efficiency. However, compared to [41]’s graph structure inference, our linear probing setting ensures the minimum time overhead, also with better performance. For making model decisions during deployment, to pursue the trade-off between performance and speed, UrbanVLP is the optimal choice.

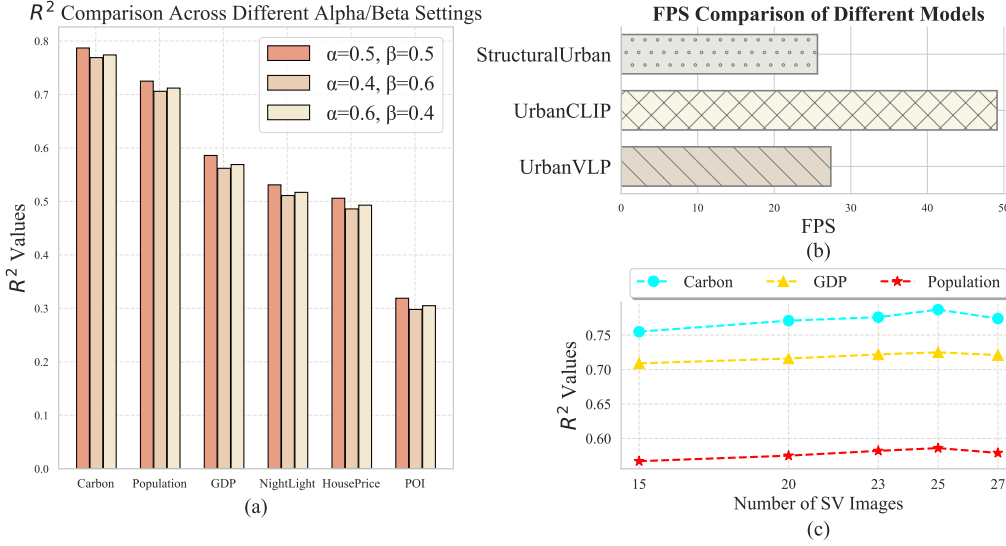


Figure 16: (a) Hyperparameter for loss combination. (b) FPS comparison of different models. (c) Experiments for maximum of the number of street-view images.

H.3 Analysis about Hyperparameters

The optimal hyperparameters for Equation 7 are actually determined by grid search. In Figure 16(a), we present some results of different combinations of hyperparameter values. It can be seen that the settings we chose in the paper ($\alpha=0.5, \beta=0.5$) yield the best experimental results.

We also study the maximum value of street-view images during training, which is set as 25 in our paper. As is shown in Figure 16(c), as the number of street-view images increases, the R^2 value continuously rises, reaching its peak at 25. Therefore, our setting is the optimal choice.

I Practicality

To demonstrate the practical applications of our model in real-life scenarios, we have developed a system bearing the same name UrbanVLP. The UrbanVLP system is a novel web-based system developed to integrate LMMs with a multi-scale urban indicator framework using the Mapbox platform [56]. This system renders a visual representation of urban areas through satellite imagery, complemented by street-level photographs for an interactive exploration experience. Figure 17 showcases the user-friendly interface of the map, highlighting functionalities that facilitate zooming, searching for locations, and navigating through various sectors.

Each urban region captured by a satellite image, encompassing a $1\text{km} \times 1\text{km}$ area, is marked by a blue dot, which is encircled by yellow points that denote the locations of street-view images accessible within that region. Engaging with these points allows users to uncover a suite of urban metrics, such as carbon emissions, population, GDP, night light, house price, and POI. The system’s visual components are augmented by a captioning feature that provides clear and informative textual descriptions, offering insights into the spatial characteristics of the designated area.

Furthermore, a street-view panel allows users to peruse individual street-view images alongside pertinent captions. The system also facilitates the discovery of popular POIs within any given area, enriching the understanding of its functional characteristics. Ultimately, UrbanVLP is designed to distill complex urban data into a visual and user-friendly format, thereby offering a holistic and detailed view of urban landscapes and their key indicators.

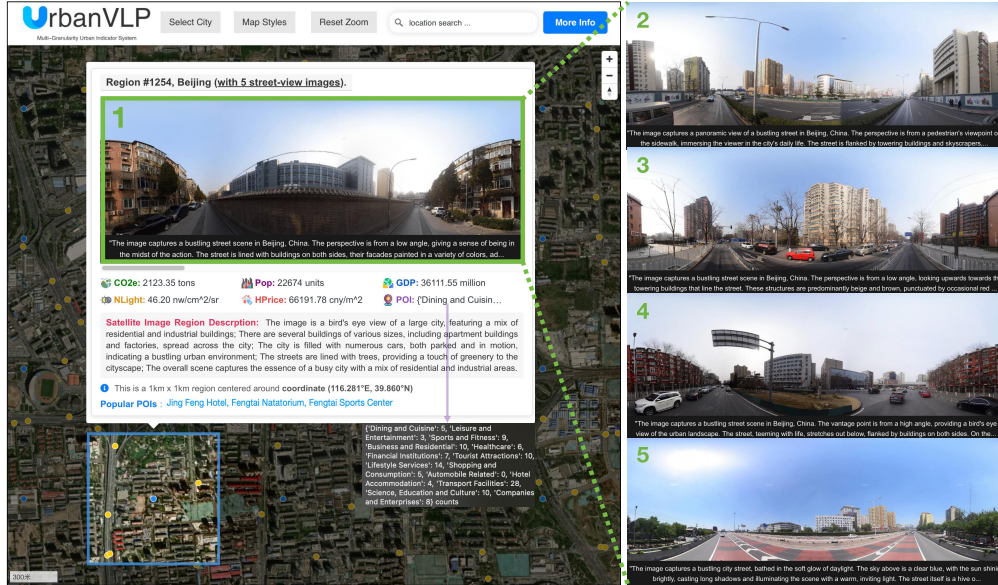


Figure 17: UrbanVLP system.

J Limitations and Social Impact

Due to the easier accessibility of the dataset, our work primarily focuses on first-tier and domestic cities, which introduces a certain bias and can be regarded as a limitation of our study. Moreover, the model's performance is significantly influenced by image resolution; higher quality image data is required to achieve optimal performance. Additionally, the introduction of new modalities inevitably leads to a decrease in inference efficiency, which should be a consideration for practical deployment. Moreover, the inability to automatically correct low-quality text highlights an area for future improvement.

Our work can be deployed in practical applications, as demonstrated by the example provided in the paper, thereby aiding urban planning and decision-making processes. However, it is crucial to note that satellite and street-view images might inadvertently contain private information. The street-view images we collected have been blurred by the Baidu Map to obscure relevant information, such as license plates, thereby significantly reducing associated risks. Nevertheless, we strongly advise users to perform a comprehensive analysis of the data prior to deploying our model in practical contexts.